Porous mullite ceramics with low thermal conductivity prepared by foaming and starch consolidation

Lunlun Gong · Yonghong Wang · Xudong Cheng · Ruifang Zhang · Heping Zhang

Abstract Porous mullite ceramics were prepared from an industrial grade mullite powder by foaming and starch consolidation. The viscosities of the original suspensions and the foamed ones with solid loading of 62.5 and 67.5 wt% were measured. After the steps of forming and drying, the green bodies were sintered under different temperatures from 1,200 to 1,600 °C for 2 h. The influence of solid loading of suspension and sintering temperature on the porosity and compressive strength was evaluated. The sintered mullite ceramics, with porosity from 86 to 73 vol% and corresponding compressive strength from 1 to 22 MPa, contained a multi-modal microstructure with large spherical pores and small pores on internal walls. Thermal conductivity measurement carried out by the transient plane source technique at room temperature resulted in values as low as 0.09 W/mK. In addition, the relationship between thermal conductivity and porosity was discussed in detail.

Keywords Mullite · Porosity · Thermal conductivity · Porous ceramics

1 Introduction

Nowadays there are great attentions on porous ceramics for their widespread industrial applications in filters, membranes, catalyst supports, solid oxide fuel cells, thermal insulation and so on, as a result of their specific properties, such as low bulk density, low thermal conductivity, heat resistance, high porosity and high surface area [1]. When they are used for thermal insulation, the thermal conductivity becomes a key property, less than 0.2 W/mK being usually required. To achieve a low thermal conductivity, the materials should contain a large pore volume fraction, namely high porosity [2–4]. Up to now, the reported methods for preparing highly porous ceramics are not cost-effective, and they are not suitable for large-scale industrial production. In order to reduce the fabrication cost, cheaper raw materials and economic preparation methods should be pursued.

Mullite is one of ceramic materials suitable for thermal insulation because of its excellent properties such as low thermal conductivity, sufficient mechanical strength, moderate thermal expansion coefficient, good resistance to thermal shock, good chemical durability, high melting point and excellent creep resistance [5]. Over decades of years, a number of processing routes have been developed in the interest of preparing porous mullite ceramics with high porosity, including leaching method [6], gelcasting [7], reaction-bonding technique [8], starch consolidation method [9], gel freeze drying [10] and foam-gelcasting [4]. In spite of these preparation efforts for highly porous mullite ceramics, porous mullite ceramics with both low cost and low thermal conductivity cannot be prepared by above methods. Recently, Mao et al. [11] described a foaming and starch consolidation method for highly porous ceramics. The novel processing route comprises foaming of a ceramic/starch composite suspension and subsequent consolidation of the foam. The technique which combines the merits of foaming method [12] and starch consolidation method [13] not only can prepare highly porous

L. Gong · X. Cheng · R. Zhang · H. Zhang (✉)
State Key Laboratory of Fire Science,
University of Science and Technology of China,
Hefei 230027, Anhui, People's Republic of China
e-mail: zhanghp@ustc.edu.cn

Y. Wang
School of Materials Science and Engineering,
Hefei University of Technology, Hefei 230009,
Anhui, People's Republic of China

ceramics, but also is economical, practical and environment friendly.

In present work, porous mullite ceramics were prepared with porosity ranging from 73 to 86 vol% from an industrial grade mullite powder by foaming and starch consolidation, and a relatively low thermal conductivity was achieved. Furthermore, the variation in the thermal conductivity of porous mullite as a function of porosity has been analyzed.

2 Experimental

2.1 Materials

An industrial grade fused mullite powder (200 mesh, Henan, China) was used as raw material. Figure 1 illustrates the XRD pattern of as-received mullite powder. As shown in Fig. 1, the major crystalline phase is mullite ($3Al_2O_3 \cdot 2SiO_2$, PDF #15-0776) and cristobalite (SiO_2, PDF #39-1425) exists as a minor crystalline phase. Ammonium citrate tribasic (CP-grade, Shanghai Chemical Regent Co., China) was used as dispersant. Sodium carboxymethyl cellulose (CMC, CP-grade, Shanghai Chemical Regent Co., China) was employed to stabilize the foams. Sodium dodecyl sulfate (SDS, CP-grade, Shanghai Chemical Regent Co., China) was selected as foaming agent. A corn starch (Shandong, China) was used to consolidate the foams.

2.2 Preparation processing

The foaming and starch consolidation technique typically consists of preparing a ceramic suspension, foaming, consolidation, drying and sintering, which is described in Fig. 2. Suspensions with 62.5 and 67.5 wt% solid loading, including mullite powders, some dispersants, 10 wt% corn
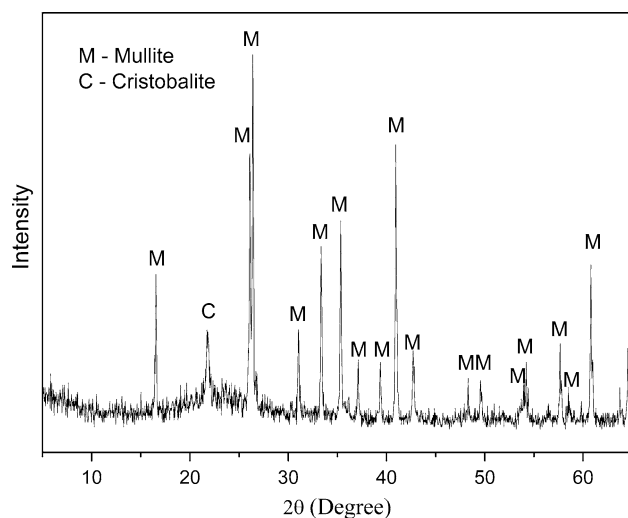
starch and 0.2 wt% CMC based on mullite powders were prepared by a planetary mill (SFM-2, China) using agate balls in a nylon pot for 20 min. By adding the foaming agent SDS (0.4 wt% of suspension), foaming of suspension was performed by a high speed stirrer operated at 800 rpm in a beaker, normally lasting for 3 min. After foaming, the foams were immediately poured into molds. Then the filled molds were moved into an 75 °C oven for 1 h. After completed drying, the sintering was performed in a programmable electric furnace (KSL-1700A2, China) under different temperatures from 1,200 to 1,600 °C for 2 h.

2.3 Characterization

The as-received mullite powder was characterized using XRD (Philips X'Pert Pro Super, Philips, Netherlands) (see Fig. 1). The viscosities of the original and foamed suspension were measured by a digital rotary viscometer (NDJ-5S, Shanghai, China). The thermogravimetry and differential thermal analysis (TG–DTA, SDTQ600, TA instrument Co., USA) of the dried green body were carried out to understand the thermal evolution of sample in air from 20 to 1,200 °C at a heating rate of 10 °C/min. The porosity of sintered sample was measured according to Archimede's method taking the theoretical density of mullite as 3.16 g/cm^3. Microstructure was observed by a digital camera (IXUS245, Canon, Japan) and a scanning electron microscope (SEM, XL30, Philips, Netherlands). The average pore size (d_{av}) was obtained using an image analyzer (Nano Measurer). The thermal conductivity of sintered sample was measured using a hot-disk thermal analyzer (TPS2500s, Hot disk AB Co., Sweden) at room temperature. Compressive strength was measured using an universal testing machine (E3000K8953, Instron Co., USA) with a crosshead speed of 0.05 mm/min. The dimension of the test piece was Φ 20 mm × 20 mm. The cross-sectional area of the sample and the maximum failure load were used to calculate the fracture stress.

3 Results and discussion

3.1 Foaming of suspensions

Because the rheological property of suspension exerts a dramatic influence on the ability of foaming and stability of foam, it is necessary to measure the viscosities of suspensions before and after foaming. The viscosities of the original and foamed suspension were measured by a digital rotary viscometer NDJ-5S. The instrument has been widely used to measure the liquid viscosity in many applications, such as grease, painting, pharmacy and so on. Comparing with other instruments, it has some advantages, including

Fig. 1 XRD pattern of as-received mullite powder

Fig. 2 Flowing-chart of process for porous mullite ceramic prepared by foaming and starch consolidation
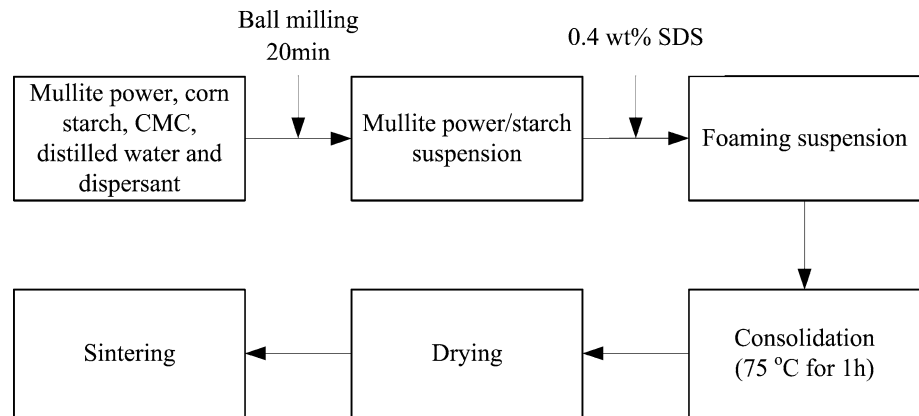
high accuracy, stable display, easy operation and read-out and excellent in anti-interference. The instrument is designed with four rotors (1#, 2#, 3#, 4#) and four rotational speed (6, 12, 30, 60 rpm). In this paper, the viscosities of the original and foamed suspension were measured within a plastic container using 2# rotor.

Figure 3 shows the viscosities of suspensions with solid loading 62.5 and 67.5 wt% before and after foaming. It can be seen that both suspensions before foaming appeared a clear pseudoplastic behavior, which is a typical behavior of concentrated ceramic suspensions. In the fabrication of ceramic foams, a slight pseudoplasticity can favor the generation of the foam since lower viscosities are obtained under shearing, and can significantly improve the foam stability since the viscosity increase under static conditions delays the collapse of fluid films around the bubbles [14]. On the other hand, the foaming volume which will directly determine density of green body is sensitively affected by the viscosity of suspension. It could be considered that higher solid loading results in larger viscosity and lower foaming volume. In Fig. 3 it can also be confirmed that the viscosity of the foamed suspension is much higher than the original one at low rotational speed. It can be attributed to the presence of bubbles and surfactant molecules at the gas–liquid interfaces [11]. A high viscosity of foamed suspensions at low rotational speed is advantageous to stabilize foams, but if the viscosity is over high, it is disadvantageous for casting.

3.2 Thermal evolution behaviors

In order to confirm an optimal temperature rising curve for the green body, a thermal analysis was carried out. Figure 4 shows the TG and DTA curves of a dried green body in air from 20 to 1,200 °C at heating rate of 10 °C/min. Firstly, water was removed from 20 to 100 °C with approximately 1 wt% weight loss. When the temperature exceeds 100 °C, there are two distinguished exothermal stages corresponding to two weight loss processes in the
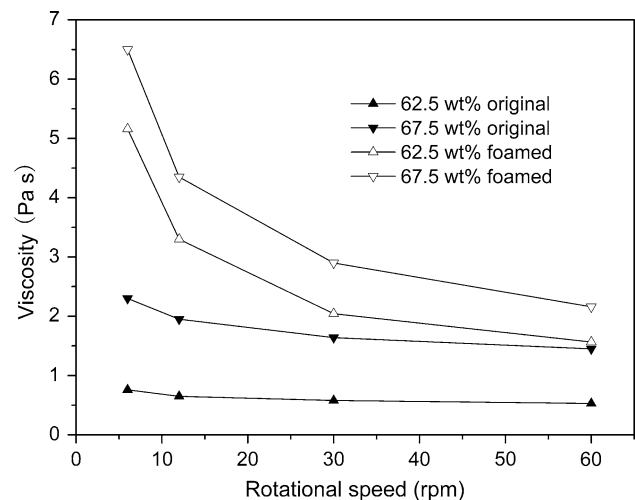

Fig. 3 Viscosities of suspensions before and after foaming

temperature range of 200–500 °C: the first stage around 329 °C with 7 wt% weight loss, and the second one around 423 °C with about 3 wt% weight loss. At these two stages, heating rate should be slow enough to avoid cracking. Based on this result, the optimal temperature rising curve for sintering green body is determined in Sect. 2.2.

3.3 Porosity

The effect of sintering temperature on the porosity of sintered samples is illustrated in Fig. 5. As shown in Fig. 5, for 62.5 wt% solid loading the porosity of porous mullite ceramics decreases from 86.33 to 76.21 vol% with the increasing sintering temperature, and for 67.5 wt% solid loading it decreases from 83.76 to 72.67 vol%. It can also be observed in Fig. 5 that at the same sintering temperature low solid loading sample has a higher porosity. The fact is resulted from low suspension viscosity and hence increasing foaming capacity. In addition, when sintering temperature exceeds 1,500 °C, the porosity drops more rapidly due to densification. Therefore, to gain highly
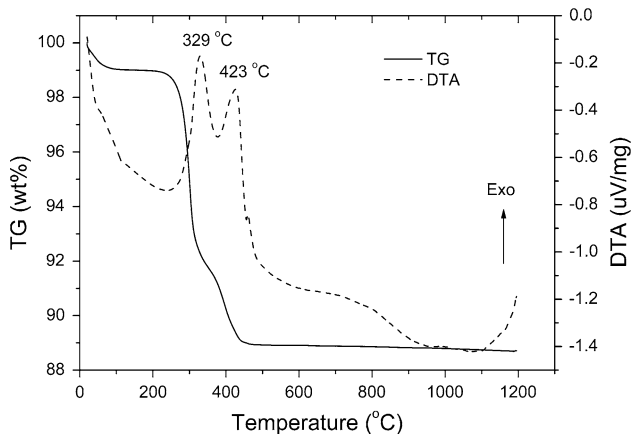
Fig. 4 TG and DTA curves of a dried green body in air

porous mullite ceramic sintering temperature should not exceed 1,500 °C.

3.4 Microstructure

Generally, the properties of porous ceramics prepared by direct foaming method are remarkably affected by pore morphology and size [15]. Figure 6a shows cross-sectional views of prepared mullite ceramics sintered at same temperature with different solid loading. By magnifying an 1×1 cm^2 area for two samples respectively, it can be observed that the two samples exhibit almost a same pore morphology, namely spherical pores with no preferred orientation, which is a typical result of direct foaming method [16]. As illustrated in Fig. 6b and c, it can also be found that higher porosity sample contains more large pores than lower one. The result indicates that the porous mullite ceramics prepared by this method exhibit a similar pore morphology and contain more large pores with higher
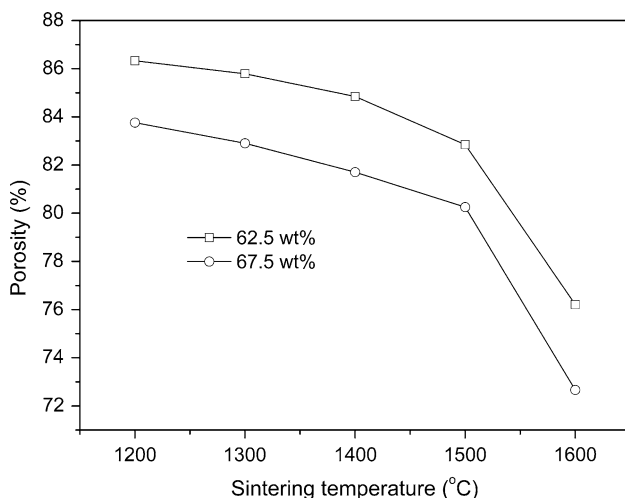

Fig. 5 Porosity of porous mullite ceramics sintered at different temperatures

porosity. In order to further validate the opinion, SEM micrographs of prepared mullite ceramics with porosity of (a) 85.79 vol% (62.5 wt%, 1,300 °C, $d_{av} = 200$ μm), (b) 82.85 vol% (62.5 wt%, 1,500 °C, $d_{av} = 170$ μm) and (c) 80.25 vol% (67.5 wt%, 1,500 °C, $d_{av} = 150$ μm) are showed in Fig. 7. The prepared mullite ceramics with different porosities display a similar pore morphology and possess a lager average pore size for higher porosity. A detailed pore microstructure of sintered mullite ceramics is illustrated in Fig. 7d, where small-sized pores locate in the internal walls of large-sized pores. It is considered that the large spherical pores were generated by foaming process, and the small pores on internal walls were derived from the organic matter removal and the particles accumulation.

3.5 Thermal conductivity

The thermal conductivity measurement was carried out by transient plane source (TPS) technique at room temperature. The main advantages of the technique include: wide thermal conductivity range (0.005–500 W/mK); wide range of materials types; easy sample preparation, non-destructive measurement; and high accuracy [17]. Figure 8 shows a sketch diagram of the hot disk system. The principal electrical circuit for the TPS technique developed by
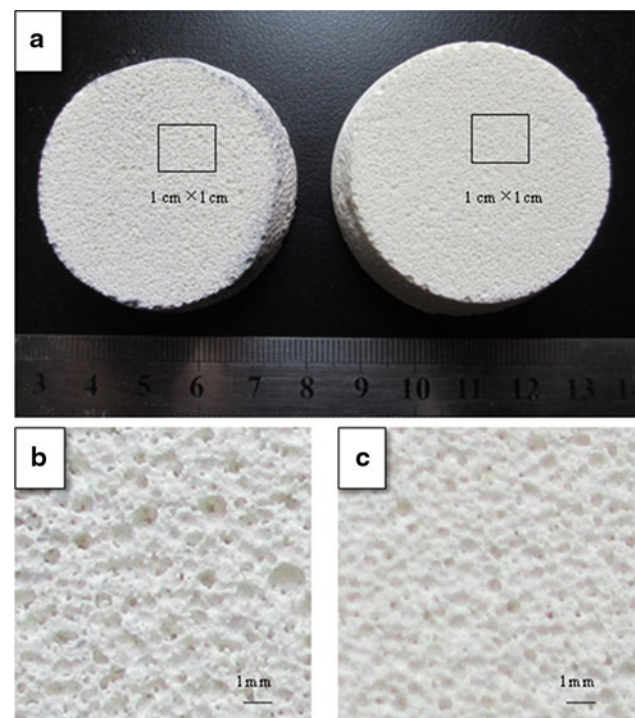

Fig. 6 a Cross-sectional views of sintered mullite ceramics sintered at 1,500 °C with solid loading of 62.5 wt% (*left*, 82.85 vol% porosity) and 67.5 wt% (*right*, 80.25 vol% porosity); **b** a magnified 1×1 cm^2 area for the left sample; **c** a magnified 1×1 cm^2 area for sample of the right sample
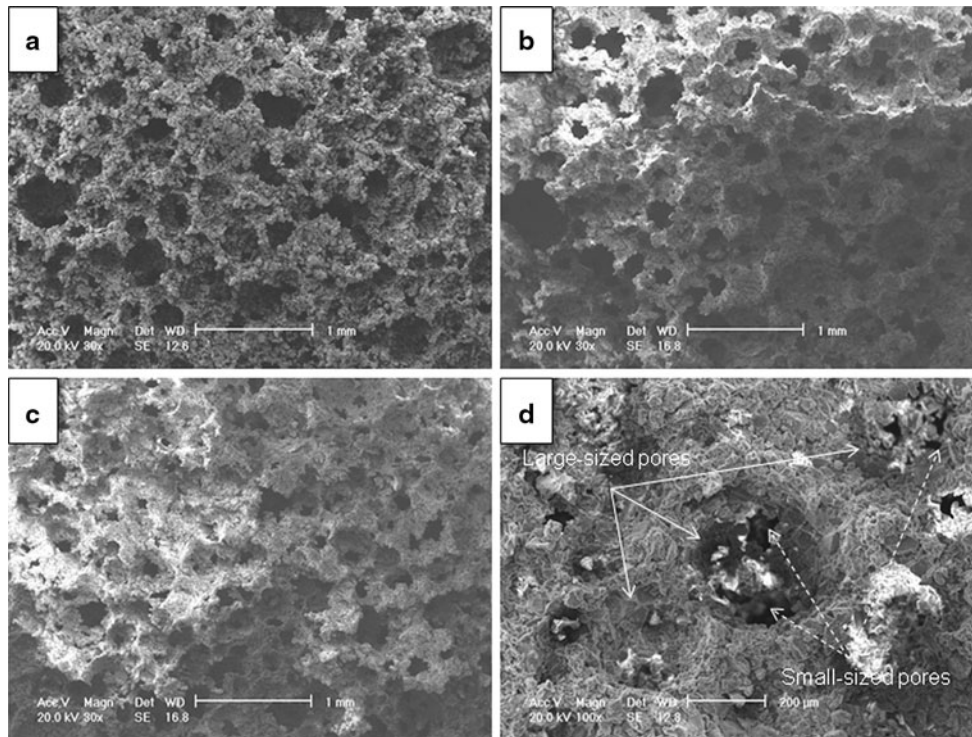
Fig. 7 SEM micrographs of sintered mullite ceramics with porosity of **a** 85.79 vol% (62.5 wt%, 1,300 °C), **b** 82.85 vol% (62.5 wt%, 1,500 °C) and **c** 80.25 vol% (67.5 wt%, 1,500 °C) and **d** a detailed pore microstructure of sintered mullite ceramics

Gustafsson [18] involved an electrical bridge. In this electrical bridge, V is the constant voltage source, U_1 and U_2 are the precision voltmeters, R_s is the constant serial resistance, R is the nonlinear resistance used simultaneously as a heat source and as a temperature sensor when measuring thermal properties of the test specimens. In the measurement, the hot disk sensor is placed between the plane surfaces of two sample pieces, and the form of samples can be arbitrary as long as the distance from the hot disk to the nearest sample boundary is larger than the probing depth during the measurement. Each pair samples were measured three times to determine the average thermal conductivity.

A porous solid can be considered as a two-phase system, viz. a dense solid skeleton and air, and its effective thermal conductivity describes heat transfer through this complex system [19]. There are many analytical models already proposed to understand the effect of porosity on the thermal conductivity of a two-phase material system, including the Maxwell–Eucken models and effective medium theory (EMT) equation [4]:

$$k_e = k_1 \frac{2k_1 + k_2 - 2(k_1 - k_2)v_2}{2k_1 + k_2 + (k_1 - k_2)v_2} \quad \text{(Maxwell - Eucken 1)}$$

$$(1)$$

$$k_e = k_2 \frac{2k_2 + k_1 - 2(k_2 - k_1)(1 - v_2)}{2k_2 + k_1 + (k_2 - k_1)(1 - v_2)}$$

$$(2)$$

$$\text{(Maxwell - Eucken 2)}$$

$$(1 - v_2)\frac{k_1 - k_e}{k_1 + 2k_e} + v_2\frac{k_2 - k_e}{k_2 + 2k_e} = 0 \quad \text{(EMT)}$$

$$(3)$$

where k and v are thermal conductivity and volume fraction, and subscripts of e, 1 and 2 represent the two-phase material system, component 1 and component 2, respectively. For the porous mullite ceramic, it consists of a dense mullite ceramic skeleton and air. For the thermal conductivity of air, a literature value equal to 0.026 W/mK was used [3]. Because of different samples or measuring method there is not a uniform value for the thermal conductivity of dense mullite materials at room temperature in the literatures [5, 20–22]. Taking into account the range of experimental thermal conductivity values (from 5.1 to 7.0 W/mK) for dense mullite, the thermal conductivity of a fully dense sample was chosen as 5.2 W/mK in present work.

As shown in Fig. 9, it can be found that the thermal conductivity of porous mullite ceramic decreases from 0.416 to 0.092 W/mK with porosity increasing from 72.67 to 86.50 vol%. Besides, the experimental data are between the Maxwell–Eucken 1 and EMT equation. The result is

Fig. 8 A sketch diagram of the hot disk system
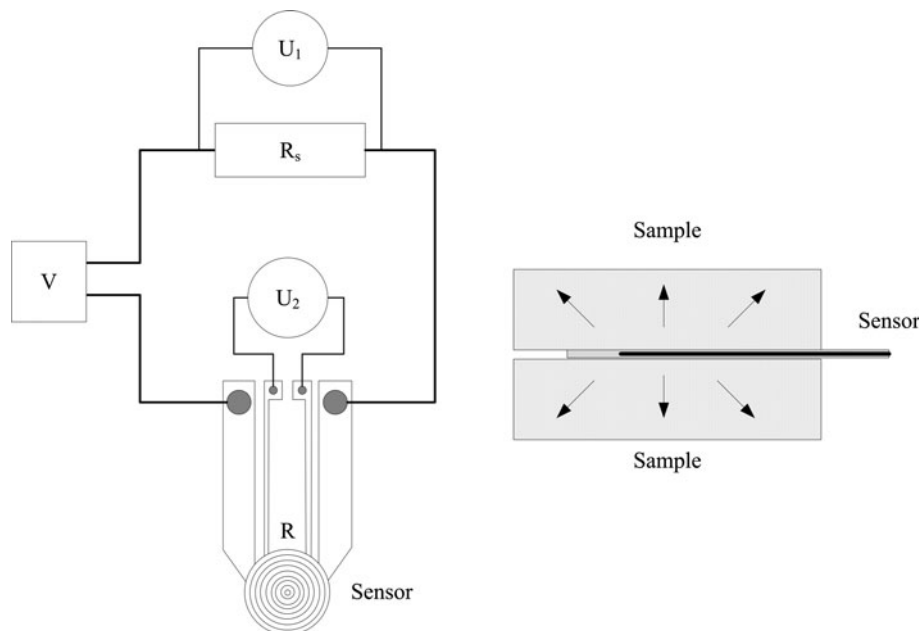
attributed to the effective thermal conductivity for a two-phase system depending on not only pore volume but also pore microstructure. Carson et al. [23] proposed that isotropic porous materials could be divided into "internal porosity" materials (e.g. sponges and foams) and "external porosity" materials (e.g. grains and particulates), according to the different heat conduction mechanism in them. Subsequently, it is validated that the effective thermal conductivity of an internal porosity material is bounded between the Maxwell–Eucken 1 and EMT equation (internal porosity region in Fig. 9) and the effective thermal conductivity of an external porosity material is bounded between the Maxwell–Eucken 2 and EMT equation (external porosity region in Fig. 9) in Carson's [23] work. For the porous mullite ceramics prepared in present work, they can be defined as "internal porosity" materials, in which condensed phase forms continuous conduction pathways. As shown in Fig. 9, the experimental data all lie in internal porosity region, agreeing well with Carson's conclusion.

Through the above analysis, it can be confirmed that the thermal conductivity of porous materials is strongly influenced by both porosity and microstructure that are significantly determined by different fabrication methods. The foaming and starch consolidation method used in present work can prepare highly porous ceramics with a lower thermal conductivity than most of processes. Moreover, the thermal conductivity of the most porous sample approaches 0.09 W/mK, it is relative low among the reported results. Furthermore, because of "internal porosity" microstructure, the samples keep a suitable mechanical strength.
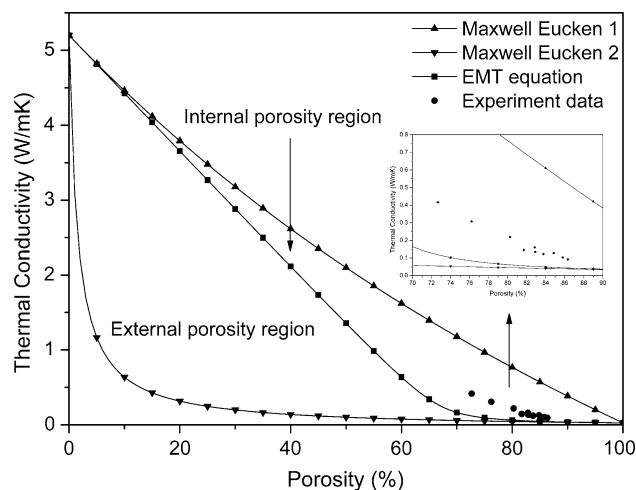

Fig. 9 Thermal conductivity as a function of porosity for experimental results and theoretical values from the Maxwell–Eucken models and the EMT equation

3.6 Mechanical strength

Figure 10 shows the compressive strength of porous mullite ceramics sintered at different temperatures. For 62.5 wt% solid loading the compressive strength of porous mullite ceramics increases from 1.02 to 13.61 MPa with the increasing sintering temperature, and for 67.5 wt% solid loading it increases from 2.14 to 22.38 MPa. Two factors could influence the mechanical strength of porous mullite ceramics prepared in this work: porosity and sintering neck. From 1,200 to 1,500 °C, the compressive strength increases slightly because the effect of porosity is
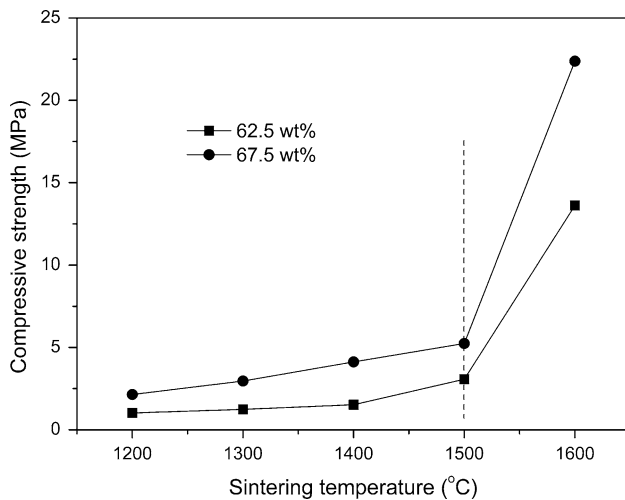
Fig. 10 Compressive strength of porous mullite ceramics sintered at different temperatures

dominant. After sintering at 1,600 °C for 2 h, the samples display a dramatic improvement of compressive strength. The result is ascribed to the increasing sintering temperature led the enhanced densification and hence increasingly strong sintering neck, resulting in dramatic increasing compressive strength.

4 Conclusions

In present work, porous mullite ceramics with low thermal conductivity (as low as 0.09 W/mK) were prepared from an industrial grade mullite powder by foaming and starch consolidation and characterized with respect to their thermal conductivities. The porosity of porous mullite ceramics can be varied from 73 to 86 vol% by adjusting solid loading of suspension and sintering temperature. The resulting porous mullite ceramics comprised a hierarchical microstructure of large spherical pores and small pores on internal walls, and possessed a larger average pore size with higher porosity. Based on the comparison of experimental thermal conductivity with analytical models (the Maxwell–Eucken models and EMT equation), it can be confirmed that the porous mullite ceramics prepared in present work can be defined as "internal porosity" materials and their thermal conductivities are located in between the Maxwell–Eucken

1 model and EMT equation. These samples prepared by foaming and starch consolidation have low thermal conductivity and meanwhile keep suitable mechanical strength. The present method has a potential engineering application value in thermal insulation.

References

1. A.R. Studart, U.T. Gonzenbach, E. Tervoort, L.J. Gauckler, J. Am. Ceram. Soc. **89**, 1771 (2006)
2. B. Nait-Ali, K. Haberko, H. Vesteghem, J. Absi, D.S. Smith, J. Eur. Ceram. Soc. **26**, 3567 (2006)
3. L. Hu, C.A. Wang, Y. Huang, J. Mater. Sci. **45**, 3242 (2010)
4. F. Yang, C. Li, Y. Lin, C.A. Wang, Mater. Lett. **73**, 36 (2012)
5. H. Schneider, J. Schreuer, B. Hildmann, J. Eur. Ceram. Soc. **28**, 329 (2008)
6. H. Abe, H. Seki, A. Fukunaga, M. Egashira, J. Mater. Sci. **29**, 1222 (1994)
7. Y.F. Liu, X.Q. Liu, H. Wei, G.Y. Meng, Ceram. Int. **27**, 1 (2001)
8. J.H. She, T. Ohji, Mater. Chem. Phys. **80**, 610 (2003)
9. R. Barea, M.I. Osendi, P. Miranzo, J.M.F. Ferreira, J. Am. Ceram. Soc. **88**, 777 (2005)
10. S. Ding, Y. Zeng, D. Jiang, J. Am. Ceram. Soc. **90**, 2276 (2007)
11. X. Mao, S. Wang, S. Shimai, Ceram. Int. **34**, 107 (2008)
12. H.X. Peng, Z. Fan, J.R.G. Evans, J.J.C. Busfield, J. Eur. Ceram. Soc. **20**, 807 (2000)
13. O. Lyckfeldt, J.M.F. Ferreira, J. Eur. Ceram. Soc. **18**, 131 (1998)
14. P. Sepulveda, J.G.P. Binner, J. Eur. Ceram. Soc. **19**, 2059 (1999)
15. P. Colombo, J.R. Hellmann, D.L. Shelleman, J. Am. Ceram. Soc. **84**, 2245 (2001)
16. X.J. Mao, S.Z. Shimai, S.W. Wang, J. Eur. Ceram. Soc. **28**, 217 (2008)
17. H. Yi, Thermochim. Acta **436**, 122 (2005)
18. M. Gustavsson, E. Karawacki, S.E. Gustafsson, Rev. Sci. Instrum. **65**, 3856 (1994)
19. B. Nait-Ali, K. Haberko, H. Vesteghem, J. Absi, D.S. Smith, J. Eur. Ceram. Soc. **27**, 1345 (2007)
20. L.M. Russell, L.F. Johnson, D.P.H. Hasselman, R. Ruh, J. Am. Ceram. Soc. **70**, C-226 (1987)
21. T.M. Kyaw, Y. Okamoto, K. Hayashi, J. Ceram. Soc. Jpn. **103**, 1289 (1995)
22. R. Barea, M.I. Osendi, J.M.F. Ferreira, P. Miranzo, Acta Mater. **53**, 3313 (2005)
23. J.K. Carson, S.J. Lovatt, D.J. Tanner, A.C. Cleland, Int. J. Heat Mass Transf. **48**, 2150 (2005)